UCID--20059

DE84 010954

RADIOCHEMICAL DETECTOR CROSS SECTION SENSITIVITY STUDIES IN THE A ≃ 90 MASS REGION

Malcolm H. MacGregor

Theoretical Physics Division
Lawrence Livermore National Laboratory, Livermore, CA 94550

ABSTRACT

The use of radiochemical detectors in the A ≃ 90 mass region to measure 14 MeV neutron fluences is investigated from the standpoint of cross section sensitivities. Specifically, ^{90}Zr and ^{89}Y neutron-induced cascades leading to the production of ^{89}Zr, ^{88}Zr, ^{88}Y, and ^{87}Y are studied in a one-energy-group approximation, and the sensitivities of the measured ratios $R_Z = {}^{88}Zr/{}^{89}Zr$ and $R_Y = {}^{87}Y/{}^{88}Y$ to the input cross sections are delineated. The most sensitive cross section in each cascade is the cross section that dominates the production of the final isotope in the chain. Only one of the isomeric levels in ^{90}Zr contributes importantly to the Zr cascade. Burnback (n,γ) and burnup (n,p) reactions are also considered. The (n,γ) effects are small, but (n,p) effects can be substantial due to low energy enhancements of (n,p) cross sections in the neutron-deficient isotopes.

I. Introduction

A problem of central interest in nuclear weapons research is the measurement of 14 MeV neutron fluences in an environment dominated by a flood of low energy fission neutrons. This measurement necessitates the use of detectors that are sensitive to 14 MeV neutrons but not to low energy neutrons. Intermediate-mass radiochemical detectors based on the (n,2n) reaction are ideal, since the (n,2n) thresholds for these isotopes lie above the bulk of the fission spectrum, and since the interfering (n,3n) thresholds lie well above the 14 MeV (D,T) peak. Sequential (n,2n) reactions can be used to monitor 14 MeV neutron fluences, since the ration of second-order (n,2n) reactions to first-order (n,2n) reactions is directly proportional to the flux. Two reaction cascades that have been used for this purpose are

$$^{89}Y \rightarrow {}^{88}Y \rightarrow {}^{87}Y \qquad (1)$$

and

$$^{90}Zr \rightarrow {}^{89}Zr \rightarrow {}^{88}Zr \quad . \qquad (2)$$

These cascades are analyzed in the present report.

In calculating the reaction sequences (1) and (2), we must consider the relevant (n,2n) and (n,n'γ) cross sections that come into play, taking into account the production of isomeric states. We should also consider the (n,γ) cross sections that lead to burnback, and the (n,p) cross sections that operate both in destruction channels and in Zr→Y cross-talk channels. Some of these cross sections have been experimentally measured, but many of them have not, since they involve unstable isotopes for which no target materials exist. In this latter case, we must resort to theoretically-calculated cross section values.

In the Y and Zr production cascades of Eqs. (1) and (2), it is important, as Poppe has emphasized,[1] to single out those reactions which tend to dominate the cascades. Poppe wrote down a general formalism[1] for evaluating the sensitivity of each branch of the cascade. In the present report we carry out a Poppe-type analysis of these cascades, but with two main simplifying assumptions: (1) the isomeric levels are considered to be stable during the irradiation process; (2) the neutron cross sections are handled in an one-energy-group approximation. Also, factors such as time dependent neutrons fluences and spatial flux gradients, which are accounted for in the Poppe formalism,[1] are not considered here.

The plan of the paper is the following. In Section II we describe the various isotopic states and cross sections that enter into the Y and Zr cascades of Eqs. (1) and (2). In Section III we consider several (n,2n) and (n,γ) cross section sets and use them to calculate the cascade ratios

$$R_Z = {}^{88}Zr/{}^{89}Zr \tag{3}$$

and

$$R_Y = {}^{87}Y/{}^{88}Y \quad , \tag{4a}$$

$$R_Y^M = {}^{87M}Y/{}^{88}Y \quad . \tag{4b}$$

In Section IV we carry out a sensitivity analysis of these cross sections. Finally, in Section V we add (n,p) and (n,γ) channels to the cascade calculations. These results are briefly summarized in Section VI.

II. The Y and Zr cascade chains

In a thermonuclear explosion, 14 MeV neutrons are produced in a single short burst. If foils of ^{89}Y and ^{90}Zr are exposed to such a burst, the isotopes ^{88}Y, ^{87}Y, ^{89}Zr, and ^{98}Zr are produced by sequential (n,2n) reactions. In considering these production processes in detail, we must include the isomeric states that are formed. These states have lifetimes that are much longer than the duration of the 14 MeV pulse, and hence appear essentially as stable levels during the course of the explosions. Figure 1 shows the isomeric levels in the yttrium isotopes, and Fig. 2 shows the isomeric levels in the zirconium isotopes. The 089 level in Fig. 1 denotes the initial Y target isotope, and the 090 level in Fig. 2 denotes the initial Zr target isotope. When these targets are exposed to a 14 MeV neutron flux, (n,n') reactions lead to population of the 389 level in Y and the 390, 490, and 590 levels in Zr. First-order (n,2n) reactions then lead to the population of the 088, 388, and 488 levels in Y and the 089 and 389 levels in Zr; and second-order (n,2n) reactions on these newly-produced isotopes lead in turn to the population of the 087 and 387 levels in Y and the 088 level in Zr. The transition channels for these Y and Z cascades are shown in Figs. 3 and 4, respectively, where they are assigned a standard set of channel numbers. In order to calculate these cascades, we must assign cross sections values for each of the channels. Since most of the levels shown in Figs. 1-4 are highly unstable, direct cross section measurements are not possible, and we must rely mainly on theoretical calculations.

In the present paper, we carry out sensitivity studies using the reaction channels shown in Figs. 3 and 4. However, for completeness, the effects of competing (n,p) and (n,γ) reactions should also be considered. These competing channels are discussed in Section V.

III. Y and Zr (n,2n) and (n,n') cross section sets.

The main purpose of the present paper is to evaluate two standard (n,2n) and (n,n') cross section sets -- Y581 and Zr280. The Y581 set is a collection of appropriate (n,2n) and (n,n') yttrium cross sections, and it was put together primary by E. D. Arthur at Los Alamos National Laboratory.[2] The Zr280 set is a similar collection of zirconium cross sections, and it was put together by workers at Lawrence Livermore National Laboratory. In the present paper, we refer to Y581 and Zr280 collectively as Data Set I.

One way to evaluate a cross section set is to compare it to an independently-produced set of cross sections. To accomplish this, we used the statistical pre-equilibium code STAPRE[3] to carry out Hauser-Feshbach-type calculations of complete sets of Y and Zr (n,2n) and (n,n') cross sections.[4] These cross sections were calculated from "first principles" -- that is, from measured levels in the various Y and Zr isotopes, but without any reference to experimental (n,2n) or (n,n') cross section values. Hence they constitute entirely independent cross sections from those contained in the Y581 and Zr280 data sets. The STAPRE code used for these calculations was obtained directly from Vienna,[5] and is generically related to similar codes now in use at Livermore[6] and Los Alamos.[2] Optical model transmission coefficients[3] for the calculations came from a code developed by Dietrich.[7] These "first principle" Y and Zr cross sections are denoted here as Data Set II.

Data Set II, as described just above, is useful only in a heuristic sense as an alternative to Data Set I for comparison purposes. We made two subsequent modifications to Data Set II, as follows.[8] First we compared the cross section values of Data Set II to the experimental data, where available, and renormalized the corresponding calculated cross sections so as to more

closely match the experimental data. This partially-renormalized data set is denoted here as Data Set III. Then we took the remaining cross sections, for which no data exist, and "artfully" renormalized them as well, using the experimental renormalizations as a guide. This fully-renormalized data set is denoted here as Data Set IV. Data Sets II, III, and IV thus serve as comparison sets to the standard Data Set I. Our goal here is to investigate the sensitivity of the calculated ratios R_Z, R_Y, and R_Y^M (Eqs. (3) and (4)) to these various choices for the input cross section sets.

Data Sets I and II initially contained cross section values that span a range of neutron energies. However, since a thermonuclear explosion produces a pulse of neutrons centered rather sharply at 14 MeV, it is a reasonable approximation to use a one-energy-group cross section for each (n,2n) and (n,n') cascade channel. To accomplish this, a computer code UNITY was written[8] that multiplies each calculated cross section by a standard neutron weighting spectrum.[9] The neutron weighting spectrum extends from 8 to 15 MeV, with a prominent peak at 14 MeV. The calculated cross sections were binned into 0.1 MeV intervels for multiplication with the weighting spectrum, and then processed with the UNITY code.

For the calculation of the Y and Zr cascades, an iterative cascade code, CASITER, was set up.[8] The procedure used in the cascade calculations is as follows: (1) a set of one-energy-group cross sections is set up that includes all of the various (n,n') and (n,2n) channels shown in Figs. 3 and 4; (2) a total integrated neutron flux value is chosen, where the pulse length is assumed to be short as compared to the isomeric lifetimes; (3) the total neutron pulse is divided into 100 subpulses; (4) the production and depletion of each level is calculated for a single subpulse; (5) step (4) is iterated over the 100 subpulses; (6) short-lived isomeric states are assumed to cascade

back down to the corresponding ground states at the end of the calculation.

Table I shows the results of the Y and Zr cascade calculations for the Data Set I cross sections (Y581 and Zr280). In each calculation, a sequence of six integrated neutron pulse values was used, ranging from target depletions of 60-70% for the largest pulse values down to essentially zero depletion for the smallest pulse values. For the Zr cascade, the ratio R_Z (Eq. (3)) is shown, and for the Y cascade both of the ratios R_Y and R_Y^M (Eq. (4)) are shown, where ^{87M}Y is a 13 hour metastable state. As can be seen in Table I, the ratios R_Z, R_Y, and R_Y^M are strictly proportional to the integrated flux for target depletions of less than 1%. These ratios exhibit 1% nonlinearities at target depletions of 10%, and they exhibit 10-20% nonlinearities at target depletions of 60-70%. Thus an accurate cascade calculation is required for target depletions of 10% or more, but not for smaller target depletions.

Table II shows the cascade results for the "first principles" Data Set II. Since this data set was not matched to experiment, it represents a "worst case" comparison. The three ratios R_Z, R_Y, and R_Y^M in Table II are 75%, 70%, and 63%, respectively, of the corresponding ratios in Table I, at the highest flux values. Thus the use of a completely theoretical set of cross sections results in errors of 25-37% in the Zr and Y R-ratios.

Table III shows the cascade calculations for the partially-renormalized Data Set III. The R-ratios R_Z, R_Y, and R_Y^M, as compared to Table I, are now 93%, 88%, and 86%, respectively, at the highest flux values. Table IV shows the cascade calculations for the fully-renormalized Data Set IV. The high-flux R-ratios, as compared to Table I, are 94%, 86%, and 85%, and the low-flux R-ratios are 96%, 90%, and 89%. (It should be noted here that the data renormalizations[8] carried out in Data Sets III and IV were made solely

with respect to the experimental cross section data, and not with the aim of making the R-ratios agree.)

The results shown in Tables III and IV are very similar to one another. Comparing the results to those of Table I, we can draw the following conclusions: (1) The high-flux Zr ratio shown in Table IV is only 6% different from the corresponding Table I ratio, and the low-flux Zr ratio differs by just 4%. Thus it is unlikely that there are any errors in the Zr280 cross section set which would lead to an error of as much as 5% in the R_Z ratio. (2) The high-flux Y ratios shown in Table IV are about 15% lower than the corresponding Table I values, and the low-flux ratios are about 10% lower. Thus it is unlikely that there are any errors in the Y581 cross section set which would lead errors of more than 10% in the R_Y and R_Y^M ratios. (There is of course no evidence from the present studies for any errors in either the Zr280 or Y581 cross section sets.) (3) The Table III and Table IV results for the R_Z, R_Y, and R_Y^M ratios are in every case lower than the corresponding Table I results. Thus if we compare the accuracy of the zirconium R-ratio with the accuracy of the yttruim R-ratios, the present analysis indicates that these are in agreement with one another at an accuracy level of 5% for low-flux results, and at an accuracy level of about 8% for very-high-flux results. Hence any discrepancies between Y and Zr determinations of 14 MeV flux values which are larger than 10% should not be ascribed to inaccuracies in the basic (n,2n) and (n,n') cross section sets.

IV. Cross section sensitivity calculations

In constructing a set of Y or Zr cascade cross sections, it is important, as Poppe has emphasized,[1] to single out the cross sections that are the most important, so they can be given the most attention. This can be accomplished with sufficient accuracy by a straight-forward single parameter sensitivity analysis. We start with the Data Set I solutions of Table I for the Y and Zr cascades of Figs. 3 and 4, and then vary each cross section value up and down so as to produce 1% increases in the calculated values for R_Z (Eq. (3)) and R_Y (Eq. (4a)). The results of this procedure for high flux values are displayed graphically in Figs. 5 and 6, and the dominant (most sensitive) reactions are summarized in Table V.

As can be seen in Fig. 5 and Table V, the (secondary) $^{88}Y(n,2n)\ ^{87M}Y$ cross section dominates the Y cascade: a 1.9% change in this cross section produces a 1% change in the $R_Y = {}^{87}Y/{}^{88}Y$ ratio. Similarly, as can be seen in Fig. 6 and Table V, the (secondary) $^{89}Zr(n,2n)\ ^{88}Zr$ cross section dominates the Zr cascade: a 1.1% change in this cross section produces a 1% change in the $R_Z = {}^{88}Zr/{}^{89}Zr$ ratio. It would seem at first glance that the primary $^{89}Y(n,2n)\ ^{88}Y$ and $^{90}Zr(n,2n)\ ^{89}Zr$ cross sections would also be dominant. However, a change in the primary $I_1 \rightarrow I_2$ cross section in a $1 \rightarrow 2 \rightarrow 3$ reaction sequence affects the amounts of both of the subsequent isotopes I_2 and I_3, whereas a change in the secondary cross section only affects the amount I_3 of the last isotope. Hence, in calculating the ratio $R = I_2/I_3$, this ratio is (roughly speaking) linearly proportional to the second-order cross section, but only proportional in a higher derivative to the first-order cross section.

As can be seen in Fig. 5, the transition to the ^{89M}Y isomeric state rather than to the ^{87}Y ground state is the dominant reaction in this cascade.

The reason for this can be ascertained by studying the level populations at the end of the neutron bombardment. These are shown for Y in Figs. 7 and 8, and for Zr in Figs. 9 and 10. As can be seen in Figs. 7 and 8, the ^{87M}Y metastable level is more heavily populated than the ^{87}Y ground state at the end of the bombardment, for both high and moderate flux levels. For the Zr cascade, on the other hand, the ^{89}Zr and ^{88}Zr ground states dominate the secondary-isotope production. At high flux levels, both the ^{89M}Y and ^{90M2}Zr metastable levels are heavily populated, and hence must be included in accurate cascade calculations.

In Table V we have summarized the sensitivities of the dominant (n,2n) cross sections in the Y and Zr cascades, and also the accuracies to which these cross sections are known experimentally. Of the 13 reaction channels shown in Table V, seven have been measured with reasonable experimental accuracy (at 14 MeV), whereas six are dependent on theoretical calculations, since they involve highly unstable levels for which no targets are available.

The sensitivities of these cross sections depend to some extent on the magnitude of the neutron flux. Table 6 shows the Y sensitivities for high, medium, and low flux values, and Table 7 shows the corresponding Zr sensitivities. Tables 6 and 7, which are based on the cascade solutions displayed in Table I, extend the results shown in Figs. 5 and 6.

The principal conclusions to be drawn from these sensitivity studies are that (1) many of the isomeric levels are only of marginal importance, and (2) we should obtain the best possible experiment values for the $^{88}Y(n,2n)$ and $^{89}Zr(n,2n)$ reactions. Fortunately, measurements of these cross sections do exist at 14 MeV,[10] and these, when combined with the theoretical calculations of M. Gardner and E. Arthur, give reasonable representations of the cross sections over the entire range of neutron energies.

V. The (n,p) and (n,γ) burnup and burnback channels.

For a complete evaluation of the Y and Zr neutron-induced cascades, (n,p) and (n,γ) cross sections should also be taken into account. Their effect on the cascades is illustrated in Figs. 11 and 12. The (n,p) reaction is essentially a burnup (removal) process, although it can cause cross talk from the Zr to Y isotopes (see Figs. 13 and 14) if both of these elements are included in the experiment. The (n,γ) reaction is a burnback process that works in opposition to the (n,2n) effect.

The difficulty in including (n,p) and (n,γ) reactions in the present studies is that, in contract to the (n,2n) reactions, many of these (n,p) and (n,γ) cross sections do not have high-energy neutron thresholds. For the nuclei ^{89}Y and ^{90}Zr, which have "normal" neutron-to-proton ratios, the (n,p) cross sections have energy dependences very similar to those of the corresponding (n,2n) reactrons. But in the cases of the neutron-deficient nuclides ^{88}Y, ^{87}Y, and ^{89}Zr (for which no (n,p) measurements exist), theoretical calculations indicate that these cross sections are enhanced at low neutron energies. The (n,γ) cross sections, which are very small at 14 MeV, are also greatly enhanced at low energies. Thus our one-energy-group calculations, which are centered at 14 MeV, may grossly underestimate the effects of these competing (n,p) and (n,γ) channels. An accurate determination of these effects in an actual experiment involves a knowledge of both the 14 MeV neutron fluxes and the low-energy fission fluxes, which is beyond the scope of the present studies. However, we can gain some measure of the importance of (n,p) and (n,γ) effects by employing one-energy-group calculations and simply increasing the magnitudes of the (n,p) and (n,γ) cross sections. Table VIII shows some typical results of this procedure for Y, and Table IX shows similar results for Zr. In Table VIII, the topmost

solution features ^{88}Y and $^{87}Y(n,p)$ cross sections based on calculations of Arthur,[11] together with the measured $^{89}Y(n,p)$ cross section, and with (n,γ) cross sections also based on calculations of Arthur.[12] The next solution has the (n,γ) cross sections all increased by a factor of 10. As can be seen in Table VIII, this change in the assumed effective values for the (n,γ) cross sections has only a small effect on the cascade calculations, since the cross sections are small. Arbitrarily increasing the $^{88}Y(n,p)$ cross section by a factor of 10 raises the Ry ratio by 5% for the high-flux case and by 0.5% for the intermediate flux case. Increasing the $^{87}Y(n,p)$ cross section by a factor of 10 decreases the R_Y ratio by 8% for the high-flux case and by 1% for the intermediate flux case. Thus (n,p) effects can be important at very high flux levels.

In Table IX, the topmost solution features (unmeasured) ^{89}Zr and $^{88}Zr(n,p)$ cross sections which are set approximately equal to the measured $^{90}Zr(n,p)$ cross section. The (n,γ) cross sections are from calculations of Arthur,[13] and have little effect on the Zr cascade. Increasing the $^{88}Zr(n,p)$ cross section by a factor of 4 in Table IX brings it into line with the calculation of Arthur,[11] and it causes a high-flux decrease in the R_Z ratio of 5%. Thus an accurate knowledge of this cross section is of some importance. Theoretical calculations[11] indicate that the $^{89}Zr(n,p)$ cross section is enhanced at lower neutron energies, whereas the ^{90}Zr and $^{88}Zr(n,p)$ cross sections are not. Increasing the ^{89}Zr (n,p) cross section in Table IX by a factor of 10 to reflect this possibility increases R_Z by 8% at high flux values and by 0.8% at intermediate flux values. Hence an accurate knowledge of this cross section is also of importance.

Table X illustrates the modifications to Table I that occur when the topmost solution of Table VIII and the second solution of Table IX are added

to the cascade calculations, with the smaller values used for the (n,γ) cross sections. A comparison of Tables I and X shows that the addition of these "reasonable" (n,p) and (n,γ) effects to the cascade calculations decreases the R_Z ratio by 5% at the highest flux value, and decreases the R_Y and R_Y^M ratios by 1.3% at the highest flux value. These results do not take into account possible low-energy neutron flux enhancements.

Figures 13 and 14 indicate the changes that occur in the Y occupation diagrams of Figs. 7 and 8 when (n,p) and (n,γ) effects are included. Figures 15 and 16 indicate the corresponding changes in the Zr occupation diagrams, as compared to Figs. 9 and 10. Figures 13 and 14 also show the cross-talk contributions from the Zr(n,p) reaction, assuming equal target loadings of ^{89}Y and ^{90}Zr, and assuming the Zr(n,p) cross section values used for Figs. 15 and 16 (see Table IX). As can be seen in Figs. 13 and 14, the cross-talk effects are small even at high flux levels.

We conclude from these studies that (n,p) effects can influence the measured Y and Zr R-ratios by a few percent at very high flux levels. (n,p) cross sections are already contained in the Zr280 and Y581 cross section sets, either explicitly or else lumped together with other "removal" cross sections. The (n,γ) effects appear to be substantially smaller than the (n,p) effects, due to the smaller overall magnitudes of the (n,γ) cross sections. However, the presence of a large thermal neutron component in the experimental flux could alter this conclusion.

VI. Summary

The neutron flux pulse from a thermonuclear explosion characteristically features a sharp 14 MeV spike superimposed on a low energy fission background. The Y and Zr radiochemical detectors are based on induced (n,2n) reactions which are dominated by the 14 MeV (D,T) spike. It is mainly these reactions that we have examined in the present study. The (n,2n) cross sections, and also the associated (n,n'γ) isomeric cross sections, appear to show consistency between the Y280 and Zr581 data sets at an accuracy level of 5-10%. Burnup effects due to (n,p) reactions are appreciable (a few percent) at the highest flux levels, whereas (n,γ) burnback effects on the (n,2n) cascades appear to be much smaller. However, an accurate evaluation of these effects cannot be done with a one-energy-group approximation to the neutron spectrum. Sensitivity studies single out the $^{88}Y(n,2n)\ ^{87}Y$ reaction as dominating the yttrium cascade, and the $^{89}Zr(n,2n)\ ^{88}Zr$ reaction as dominating the zirconium cascade (Table V). Fortunately, the cross sections for these reactions are based on a combination of theoretically-calculated shapes combined with 14 MeV experimental values to anchor the normalizations. Most of the isomeric levels in the target isotopes play only small roles in the cascade processes, even at high flux levels. (n,p) processes in zirconium can cause "cross-talk" production of yttrium isotopes if both of these target materials are present. However, as shown in Figs. 13 and 14, cross-talk effects are quite small. In cases where appreciable numbers of high-energy protons are present, (p,n) reactions in yttrium can also cause cross-talk.

The present studies are sufficient to specify the nature of the yttrium and zirconium 14 MeV-neutron-induced cascades in the case where large thermal neutron fluxes are not present. Accurate calculations when thermal neutron

effects are important should be based on a multigroup representation for the neutron spectrum.

References

1. Carl H. Poppe, UCID-19567, "General Formalism for the Study of Activation: Application to Radiochemical Detectors", Sept. 24, (1982).
2. See E. D. Arthur, Nuclear Science and Engineering 76, 137 (1980). Also see Ref. 11.
3. See M. H. MacGregor, Physical Data Group report PD 84, "STAPRE calculations of gamma ray cascades", Feb. 28 (1983).
4. M. H. MacGregor, PD 85, "STAPRE calculations of (n,2n) cross sections in the A ≈ 90 mass region", March 25 (1983).
5. M. Uhl, Acta Phys. Austriaca 31, 245 (1970); M. Uhl and B. Strohmaier, IRK 76/01 and addenda.
6. See for example D. G. Gardner and M. A. Gardner, Bull. Am. Phys. Soc. 22, 993 (1977).
7. F. Dietrich III (private communication).
8. M. H. MacGregor, PD 86, "STAPRE calculations of (n,2n) cross section ratios for Y and Zr", April 15 (1983).
9. This neutron weighting spectrum was supplied by A. Delucchi.
10. D. Nethaway, private communication.
11. See E. D. Arthur, Los Alamos informal report LA-7789-MS, "Calculation of Neutron Cross Sections on Isotopes of Yttrium and Zirconium", April (1979), Figs. 20 and 33.
12. See Fig. 18 in Ref. 11.
13. See Fig. 31 in Ref. 11.

Table I Calculation of isotopic R-ratios (Eqs. (3) and (4)) for the Y and Zr cascades of Figs. 3 and 4, plotted as functions of the integrated neutron flux ϕ, and using Data Set I (Y280 + Zr581) with a one-energy-group approximation.

ϕ n/cn^2	$^{88}Zr/^{89}Zr$ RATIO	Depletion of ^{90}Zr	$^{87}Y/^{88}Y$ RATIO	$^{87M}Y/^{88}Y$ RATIO	Depletion of ^{89}Y
10^{19}	0.2673×10^{-5}	-	0.4163×10^{-5}	0.2962×10^{-5}	-
10^{20}	0.2673×10^{-4}	-	0.4163×10^{-4}	0.2962×10^{-4}	-
10^{21}	0.2673×10^{-3}	0.1%	0.4164×10^{-3}	0.2962×10^{-3}	0.1%
10^{22}	0.2675×10^{-2}	0.9%	0.4169×10^{-2}	0.2967×10^{-2}	1.2%
10^{23}	0.2696×10^{-1}	9.0%	0.4227×10^{-1}	0.3013×10^{-1}	11.3%
10^{24}	0.3023	61.2%	0.4998	0.3608	70.0%

Table II The same plot as in Table I, but using the "first principles" STAPRE Data Set II as the cascade cross section set.

ϕ n/cn^2	$^{88}Zr/^{89}Zr$ RATIO	Depletion of ^{90}Zr	$^{87}Y/^{88}Y$ RATIO	$^{87M}Y/^{88}Y$ RATIO	Depletion of ^{89}Y
10^{19}	0.2115×10^{-5}	-	0.3068×10^{-5}	0.1959×10^{-5}	-
10^{20}	0.2115×10^{-4}	-	0.3068×10^{-4}	0.1959×10^{-4}	-
10^{21}	0.2115×10^{-3}	0.1%	0.3068×10^{-3}	0.1959×10^{-3}	0.1%
10^{22}	0.2115×10^{-2}	1.1%	0.3070×10^{-2}	0.1961×10^{-2}	1.3%
10^{23}	0.2118×10^{-1}	10.3%	0.3098×10^{-1}	0.1981×10^{-1}	12.0%
10^{24}	0.2281	66.6%	0.3496	0.2264	72.3%

Table III The same plot as in Table I, but using the partially-renomalized STAPRE Data Set III as the cascade cross section set.

ϕ n/cn^2	$^{88}Zr/^{89}Zr$ RATIO	Depletion of ^{90}Zr	$^{87}Y/^{88}Y$ RATIO	$^{87M}Y/^{88}Y$ RATIO	Depletion of ^{89}Y
10^{19}	0.2481×10^{-5}	-	0.3604×10^{-5}	0.2527×10^{-5}	-
10^{20}	0.2481×10^{-4}	-	0.3604×10^{-4}	0.2527×10^{-4}	-
10^{21}	0.2482×10^{-3}	0.1%	0.3604×10^{-3}	0.2527×10^{-3}	0.1%
10^{22}	0.2484×10^{-2}	1.0%	0.3611×10^{-2}	0.2532×10^{-2}	1.1%
10^{23}	0.2504×10^{-1}	9.2%	0.3671×10^{-1}	0.2576×10^{-1}	10.3%
10^{24}	0.2806	62.0%	0.4391	0.3093	66.3%

Table IV The same plot as in Table I, but using the fully-renomalized STAPRE Data Set IV as the cascade cross section set. Data Sets III and IV give closely-similar results.

ϕ n/cm^2	$^{88}Zr/^{89}Zr$ RATIO	Depletion of ^{90}Zr	$^{87}Y/^{88}Y$ RATIO	$^{87M}Y/^{88}Y$ RATIO	Depletion of ^{89}Y
10^{19}	0.2553×10^{-5}	-	0.3751×10^{-5}	0.2626×10^{-5}	-
10^{20}	0.2553×10^{-4}	-	0.3751×10^{-4}	0.2626×10^{-4}	-
10^{21}	0.2553×10^{-3}	0.1%	0.3751×10^{-3}	0.2626×10^{-3}	0.1%
10^{22}	0.2554×10^{-2}	0.9%	0.3753×10^{-2}	0.2629×10^{-2}	1.1%
10^{23}	0.2570×10^{-1}	9.1%	0.3782×10^{-1}	0.2654×10^{-1}	10.3%
10^{24}	0.2852	61.5%	0.4304	0.3069	66.3%

Table V The dominant (most sensitive) reaction channels in the yttrium and zirconium cascades of Figs. 3 and 4. All channels are listed in which a ±25% or less variation in the cross section would change the corresponding R-ratio (Eq. (3) or (4a)) by 1%. Also shown are the experimental accuracies at 14 MeV with which these cross sections are known. Six of the cross sections have not been measured.

Reaction	Sensitivity	Experimental Accuracy
$^{88}Y(n,2n)^{87M}Y$	± 1.9%	±8%
$^{88}Y(n,2n)^{87G}Y$	± 5.5%	∿±9%
$^{88M_2}Y(n,2n)^{87G}Y$	± 6.3%	-
$^{89}Y(n,2n)^{88G}Y$	± 6.5%	∿±13%
$^{88M_1}Y(n,2n)^{87M}Y$	±10%	-
$^{88M_1}Y(n,2n)^{87G}Y$	±11%	-
$^{89}Y(n,2n)^{88M_1}Y$	±16%	∿±15%
$^{89M}Y(n,2n)^{88M_2}Y$	±17%	-
$^{89M}Zr(n,2n)^{88}Zr$	± 1.1%	∿±5%
$^{89M}Zr(n,2n)^{88}Zr$	± 6.4%	-
$^{90}Zr(n,2n)^{89G}Zr$	±10%	∿±14%
$^{90M_2}Zr(n,2n)^{89G}Zr$	±19%	-
$^{90}Zr(n,2n)^{89M}Zr$	±22%	∿±20%

Table VI The high-flux ($\phi = 10^{24} n/cm^2$) sensitivities of Fig. 5 extended to include medium-flux ($\phi = 10^{23}$) and low-flux ($\phi = 10^{19}$) values. The isomeric channels 38, 40, 41, and 56 become completely unimportant at low flux values.

Reaction Channel	High Flux $\phi = 10^{24}$	Medium Flux $\phi = 10^{23}$	Low Flux $\phi = 10^{19}$
1	±6.5	+35,-25	+130,-82
2	±16	±26	±27
3	+60,-50	±21	±20
4	±5.5	±5.4	±5.3
5	±1.8	±2.0	±1.9
6	±12.6	±11.5	±11.4
7	±10.0	±9.2	±9.2
8	±35	±64	±68
9	±6.3	±11.3	±12.3
38	±30	+161,-100	+∞,-100
40	+275,-100	+1900,-100	+∞,-100
41	±17	+108,-100	+∞,-100
56	+61,-37	+155,-100	+∞,-100

Table VII The high-flux ($\phi = 10^{24} n/cm^2$) sensitivities of Fig. 6 extended to include medium-flux ($\phi = 10^{23}$) and low-flux ($\phi = 10^{19}$) values. Only channels 9, 10, 37, and 38 are of importance at low flux values.

Reaction Channel	High Flux $\phi = 10^{24}$	Medium Flux $\phi = 10^{23}$	Low Flux $\phi = 10^{19}$
9	±22	±26	±26
10	±10	+300,-37	+35,-22
11	+∞,-100	+5600,-100	+∞,-100
12	+100,-48	+300,-100	+∞,-100
13	+600,-100	+1560,-100	+∞,-100
17	+∞,-100	+∞,-100	+∞,-100
18	+4700,-100	+∞,-100	+∞,-100
21	+20,-17	+85,-88	+∞,-100
22	+280,-100	+2900,-100	+∞,-100
25	+1900,-95	+820,-100	+∞,-100
27	+4800,-100	+∞,-100	+∞,-100
37	±1.1	±1.2	±1.2
38	±6.4	±6.3	±6.3

Table VIII The effect of burnup (n,p) and burnback (n,γ) channels (see Fig. 11) on the yttrium cascade of Fig. 3. Calculations are done for two different sets of (n,γ) cross sections with each set of (n,p) cross sections; as can be seen, the (n,γ) cross sections have little effect on the yttrium R-ratio (Eq. (4a)). Both high (10^{24}) and medium (10^{23}) flux values are considered for each set of (n,p) cross sections. Increases in the (n,p) cross sections by factors of 10, to mock up low energy neutron effects, produce substantial effects on the R-ratio at high flux levels.

ϕ n/cm^2	$^{87}Y/^{88}Y$ RATIO	σ(n,p) barns 89	88	87	σ(n,γ) barns 89	88	87
10^{23}	4.2224	.02	.035	.06	.0015	.002	.002
10^{24}	0.4934						
10^{23}	4.2221				.015	.02	.02
10^{24}	0.4919						
10^{23}	4.2456	.02	.35	.06	.0015	.002	.002
10^{24}	0.5205						
10^{23}	4.2452				.015	.02	.02
10^{24}	0.5118						
10^{23}	4.1462	.02	.035	.6	.0015	.002	.002
10^{24}	0.4063						
10^{23}	4.1447				.015	.02	.02
10^{24}	0.4052						
10^{23}	4.1677	.02	.35	.6	.0015	.002	.002
10^{24}	0.4266						
10^{23}	4.1674				.015	.02	.02
10^{24}	0.4254						

Table IX The effect of burnup (n,p) and burnback (n,γ) channels (see Fig. 12) on the zirconium cascade of Fig. 4. The second set of (n,p) cross sections shown here (see the discussion in the text) corresponds to the results that are displayed in Table X and in Figs. 15 and 16.

ϕ n/cm^2	$^{98}Zr/^{89}Zr$ RATIO	$\sigma(n,p)$ barns 90	89	88	$\sigma(n,\gamma)$ barns 90	89	88
10^{23}	2.6958	.04	.05	.05	.001	.002	.002
10^{24}	0.3016						
10^{23}	2.6953				.01	.02	.02
10^{24}	0.3006						
10^{23}	2.6820	.04	.05	.2	.001	.002	.002
10^{24}	.02860						
10^{23}	2.6816				.01	.02	.02
10^{24}	0.2851						
10^{23}	2.7169	.04	.5	.05	.001	.002	.002
10^{24}	0.3249						
10^{23}	2.7164				.01	.02	.02
10^{24}	0.3237						
10^{23}	2.7029	.04	.5	.2	.001	.002	.002
10^{24}	0.3075						
10^{23}	2.7025				.01	.02	.02
10^{24}	0.3064						

Table X The zirconium and yttrium cascade calculations of Table I as modified by the addition of burnup and burnback channels from Table VIII (top n,p cross sections) and Table IX (second n,p cross sections).

ϕ n/cn^2	$^{88}Zr/^{89}Zr$ RATIO	Depletion of ^{90}Zr	$^{87}Y/^{88}Y$ RATIO	$^{87M}Y/^{88}Y$ RATIO	Depletion of ^{89}Y
10^{19}	0.2673×10^{-5}	-	0.4163×10^{-5}	0.2962×10^{-5}	-
10^{20}	0.2673×10^{-4}	-	0.4163×10^{-4}	0.2962×10^{-4}	-
10^{21}	0.2673×10^{-3}	0.1%	0.4164×10^{-3}	0.2962×10^{-3}	0.1%
10^{22}	0.2674×10^{-2}	1.0%	0.4169×10^{-2}	0.2966×10^{-2}	1.2%
10^{23}	0.2682×10^{-1}	9.4%	0.4222×10^{-1}	0.3009×10^{-1}	11.5%
10^{24}	0.2860	62.8%	0.4934	0.3562	70.6%

Figure 1. Isomeric levels in the yttrium isotopes. The notation 0 - -, 3 - -, 4 - -, etc. denotes the ground state, 1st isomeric state, 2nd isomeric state, etc., for the isotope whose mass number is given by the second and third digits. When tracing (n,2n) production processes that start from the 089 yttrium ground state, all of these isomeric levels should be considered.

Figure 2. Isomeric levels in the zirconium isotopes. The level notation used here is described in the caption to Fig. 1. These figures give the life-times, energies, and spins and parities of the isomeric levels.

Figure 3. Transition channels in the yttrium isotopes that are reached by (n,n') and (n,2n) reactions. The channel labeling follows a standard notation. These are the channels that are important for high energy neutron fluences.

Figure 4. Transition channels in the zirconium isotopes that are reached by (n,n') and (n,2n) reactions. The channel labeling follows a standard notation. If low energy neutrons are present in appreciable numbers, then (n,γ) burnback reactions should be added to the reactions shown here (and in Fig. 3) in order to obtain accurate isotope production ratios. Reactions such as (n,p) can cause cross talk between yttrium and zirconium production cascades.

Figure 5. Sensitivity test of the yttrium cascade, using the Y280 cross section set (see Table I). The ± number beside each reaction channel denotes the percentage by which the corresponding cross section must be raised or lowered in order to produce a 1% change in the ratio $R_Y = {}^{87}Y/{}^{88}Y$. Channel 5 is the most sensitive. Channel 40 is the least sensitive, and its removal would change the R-ratio by less than 1%. The sensitivities shown here are for the highest-flux value in Table I. Sensitivities for lower-flux values are given in Table VI.

Figure 6. Sensitivity test of the zirconium cascade (see Fig. 5 for yttrium). Channel 37 is the most sensitive. Channels 11, 13, 17, 18, 22, and 27 could be individually removed without changing the ratio $R_Z = {}^{88}Zr/{}^{89}Zr$ by as much as 1%. The sensitivities shown here are for the highest-flux value in Table I. Sensitivities for lower-flux values are given in Table VII.

Figure 7. Yttrium level-occupancies at the end of the neutron irradiation pulse for the highest-flux solution ($\phi = 10^{24} n/cm^2$) of Table I. As can be seen, the 13 hour metastable 387 level is more heavily populated than the 80 hour 087 ground state. The initial 089 target level is 70% depopulated. No burnup or burnback channels are included here (see Fig. 13).

Figure 8. Yttrium level-occupancies (see Fig. 7) for the medium-flux solution ($\phi = 10^{23} n/cm^2$) of Table I. The initial 089 target level is depopulated in this case by 11.3%. The population ratio of the 387 and 087 levels is essentially the same here as in Fig. 7. The corresponding case with burnup and burnback included is shown in Fig. 14.

Figure 9. Zirconium level-occupancies for the highest-flux solution ($\phi = 10^{24} n/cm^2$) of Table I. The initial 090 level is 61.2% depopulated. The 390 and 590 metastable levels are only of minor importance in this cascade reaction. The corresponding case with burnup and burnback included is shown in Fig. 15.

Figure 10. Zirconium level-occupancies for the medium-flux solution ($\phi = 10^{23} n/cm^2$) of Table I. The initial 090 level is depopulated by 9%. The corresponding case with burnup and burnback included is shown in Fig. 16.

Figure 11. Burnback (n,γ) and burnup (n,p) neutron reactions that affect the yttrium neutron-induced cascade of Fig. 3. In assessing the significance of these reactions, we assign the same cross section values to all isomeric levels of the same isotope.

Figure 12. Burnback (n,γ) and burnup (n,p) neutron reactions that affect the zirconium neutron-induced cascade of Fig. 4. If zirconium and yttrium foils are included in the same experiment, (n,p) reactions on zirconium can produce "cross-talk" production of yttrium isotopes.

Figure 13. Changes produced in the yttrium level-occupancies of Fig. 7 when (n,p) and (n,γ) burnup and burnback channels (top solution in Table VIII) are added to the yttrium cascade calculations. Also shown are cross-talk contributions from Zr (n,p) reactions, assuming equal yttrium and zirconium target loadings.

Figure 14. Changes produced in the yttrium level-occupancies of Fig. 8 when (n,p) and (n,γ) burnup and burnback channels are added. Also shown are cross-talk contributions from Zr(n,p) reactions.

Figure 15. Changes produced in the zirconium level-occupancies of Fig. 9 when (n,p) and (n,γ) burnup and burnback channels (Table IX) are added to the zirconium cascade calculations.

Figure 16. Changes produced in the zirconium level-occupancies of Fig. 10 when (n,p) and (n,γ) burnup and burnback channels (Table IX) are added to the zirconium cascade calculations.

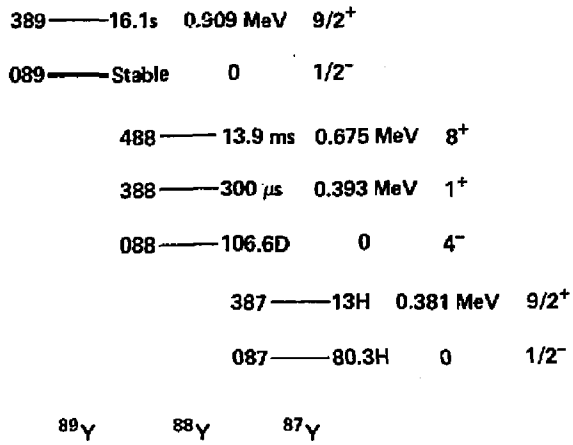
389 16.1s 0.909 MeV 9/2+
089 Stable 0 1/2−
488 13.9 ms 0.675 MeV 8+
388 300 μs 0.393 MeV 1+
088 106.6D 0 4−
387 13H 0.381 MeV 9/2+
087 80.3H 0 1/2−
89Y
88Y
87Y

Figure 1

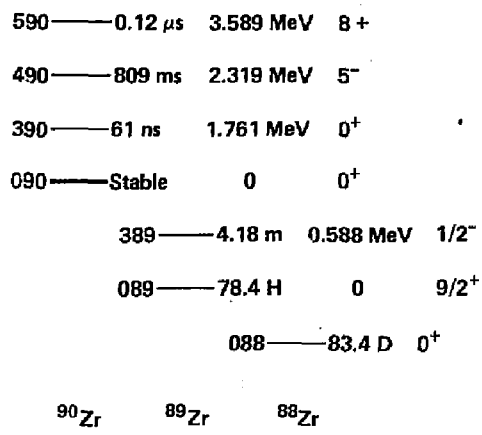
590 0.12 μs 3.589 MeV 8+
490 809 ms 2.319 MeV 5⁻
390 61 ns 1.761 MeV 0⁺
090 Stable 0 0⁺
389 4.18 m 0.588 MeV 1/2⁻
089 78.4 H 0 9/2⁺
088 83.4 D 0⁺
90Zr
89Zr
88Zr

Figure 2

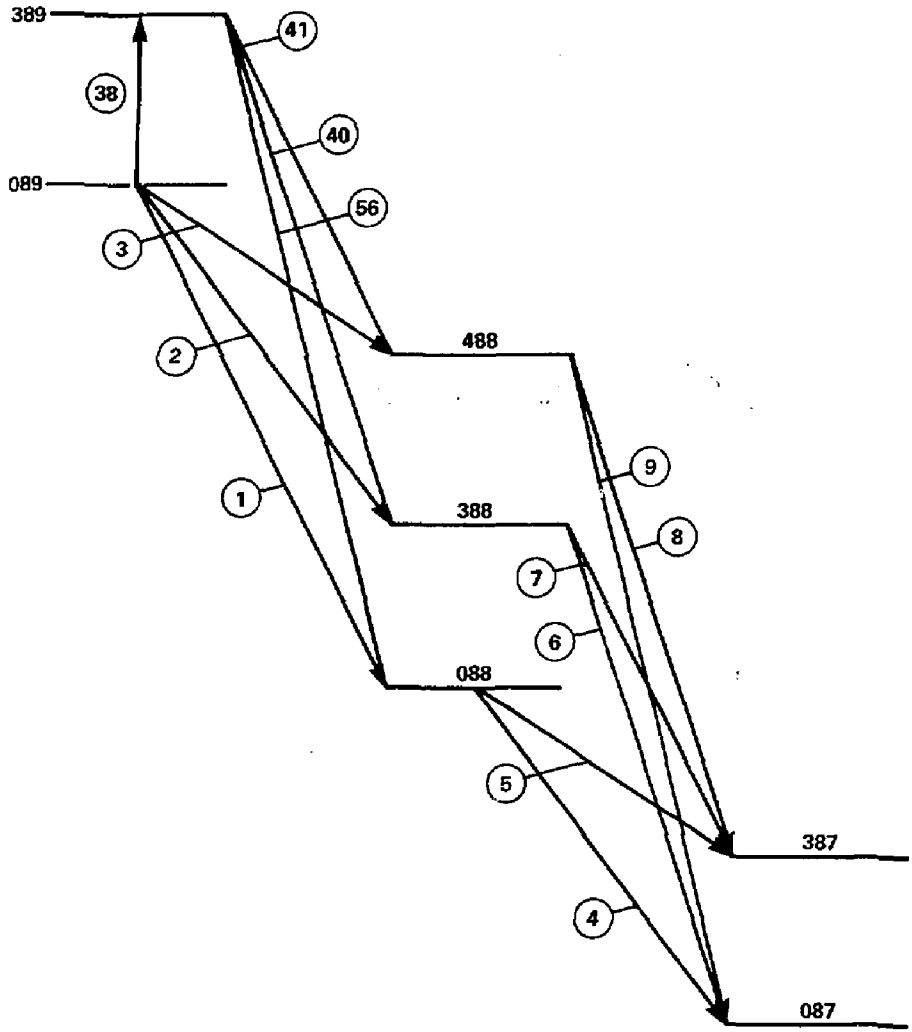

Figure 3

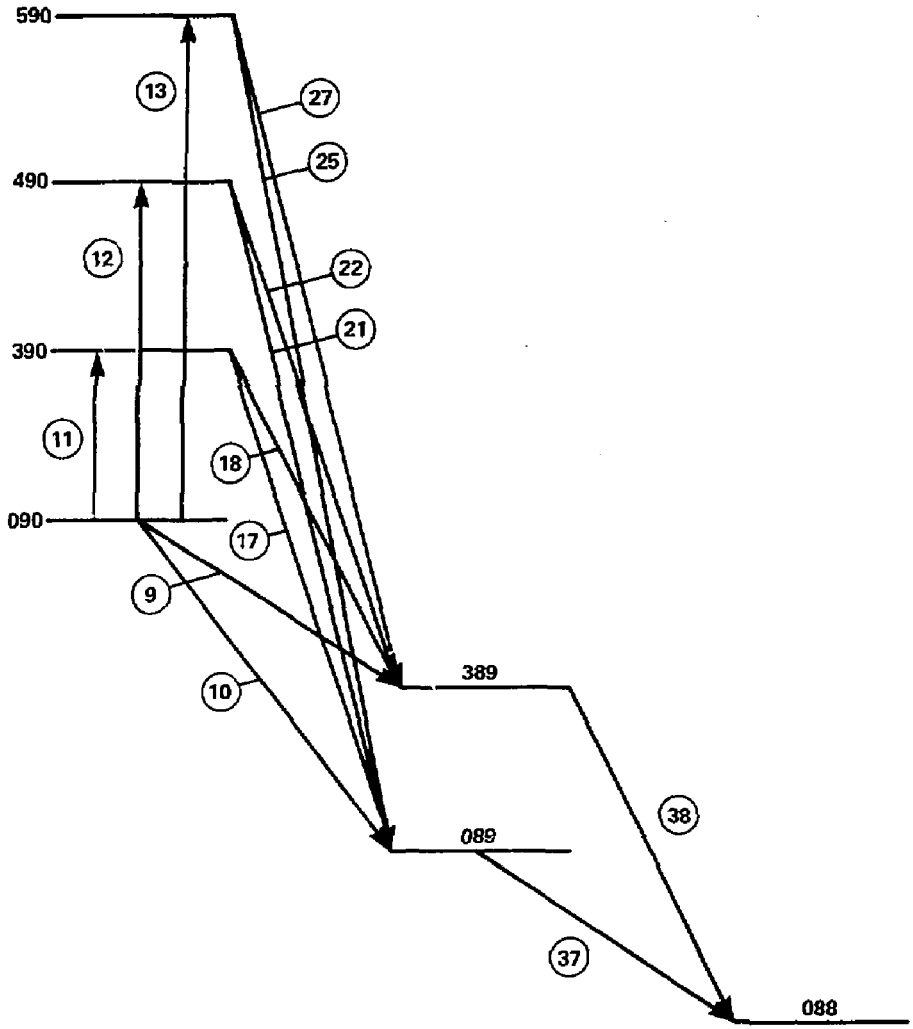

Figure 4

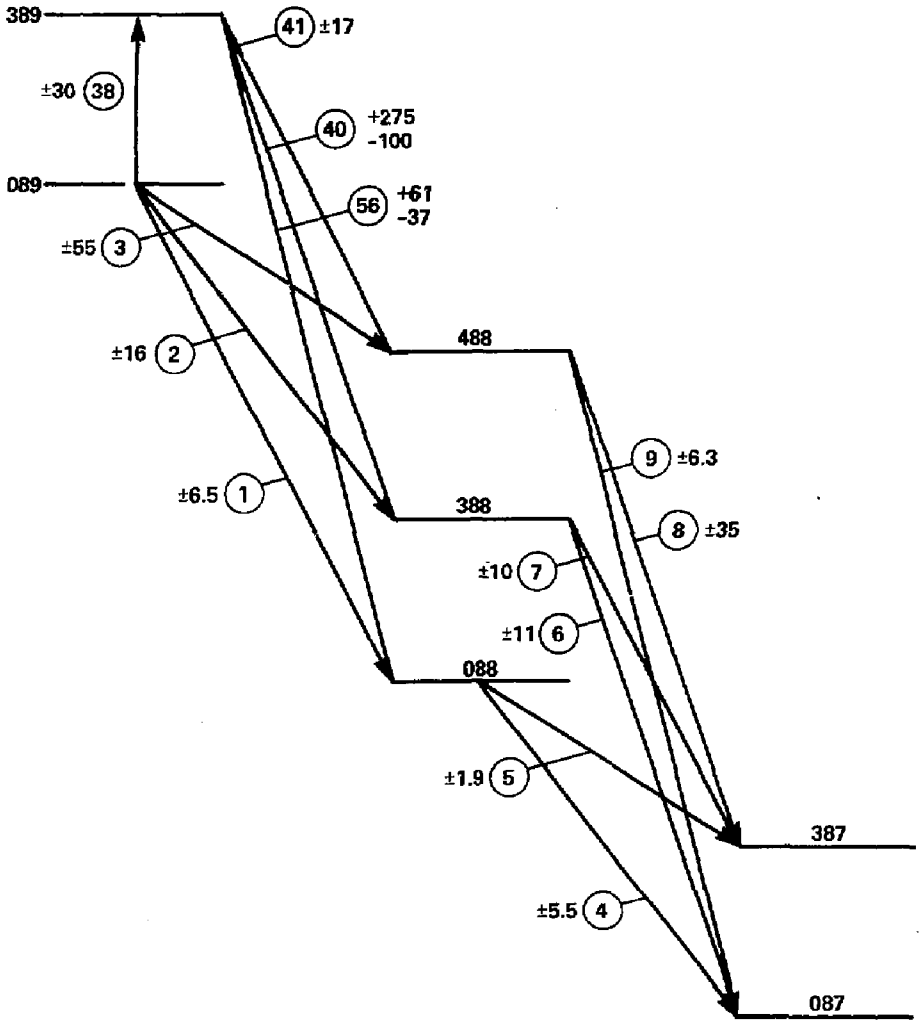
389
41 ±17
±30 38
40 +275 -100
089
56 +61 -37
±55 3
488
±16 2
9 ±6.3
±6.5 1
388
8 ±35
±10 7
±11 6
088
±1.9 5
387
±5.5 4
087

Figure 5

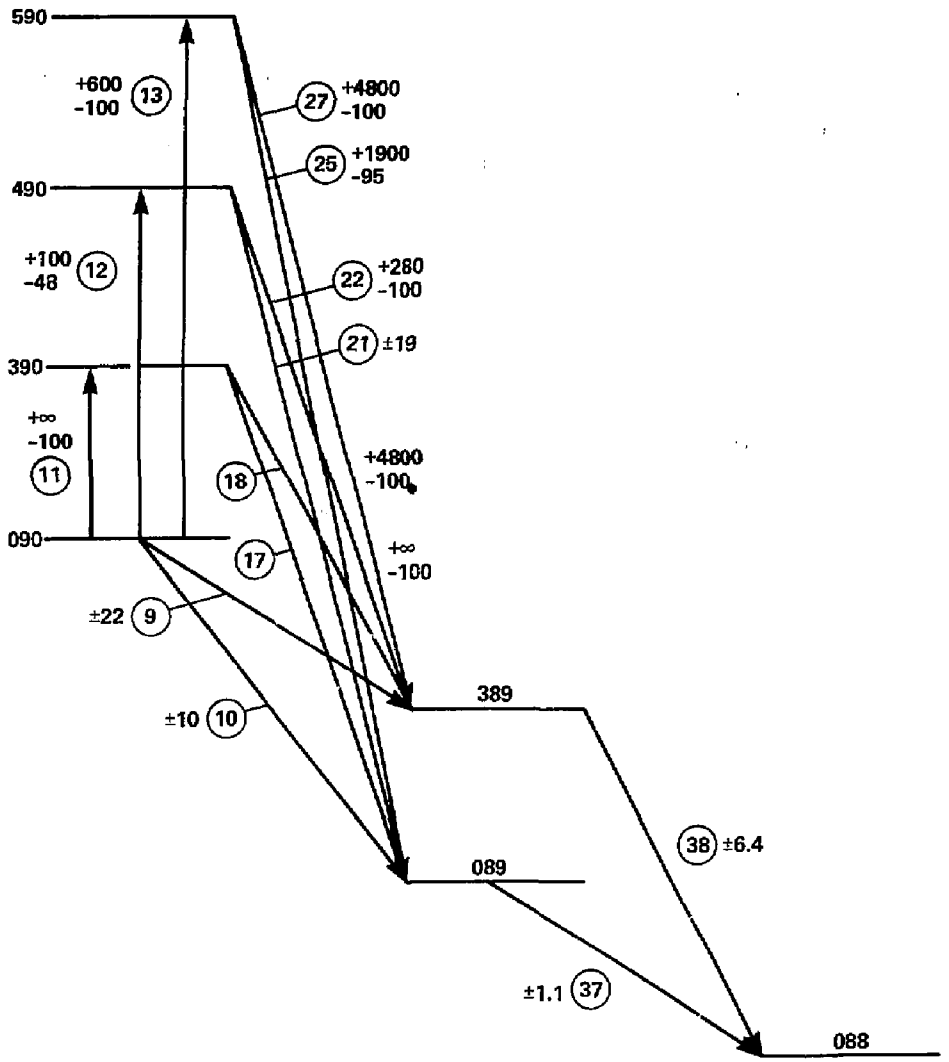
590
+600
-100
13
27
+4800
-100
25
+1900
-95
490
+100
-48
12
22
+280
-100
21
±19
390
+∞
-100
11
18
+4800
-100
090
17
+∞
-100
±22
9
389
±10
10
38
±6.4
089
±1.1
37
088

Figure 6

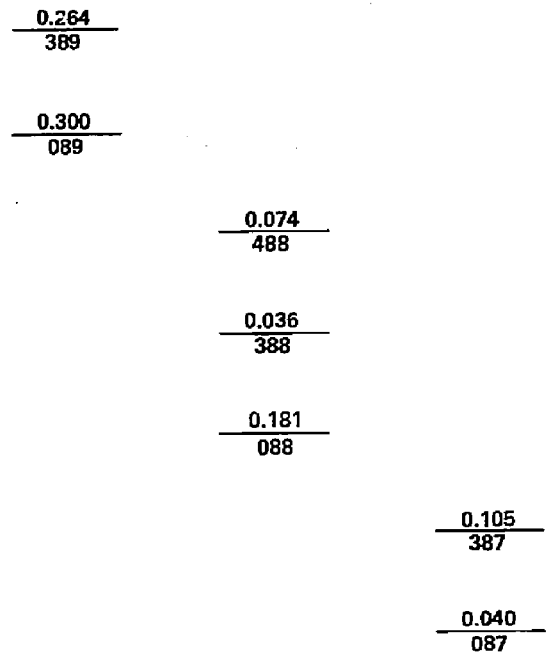

Figure 7

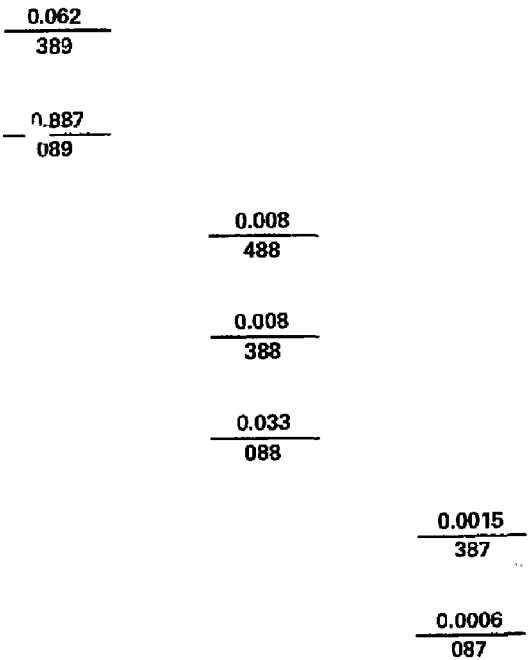
0.062
389
0.887
089
0.008
488
0.008
388
0.033
088
0.0015
387
0.0006
087

Figure 8

0.029
590

0.225
490

0.007
390

0.388
090

0.031
389

0.241
089

0.082
088

Figure 9

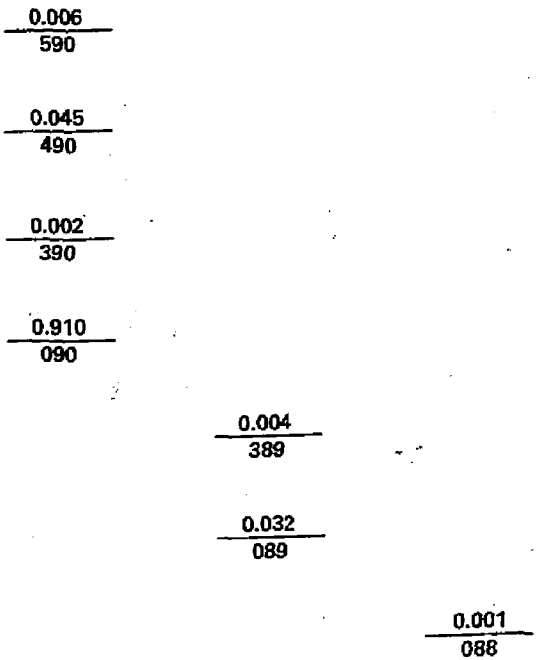

Figure 10

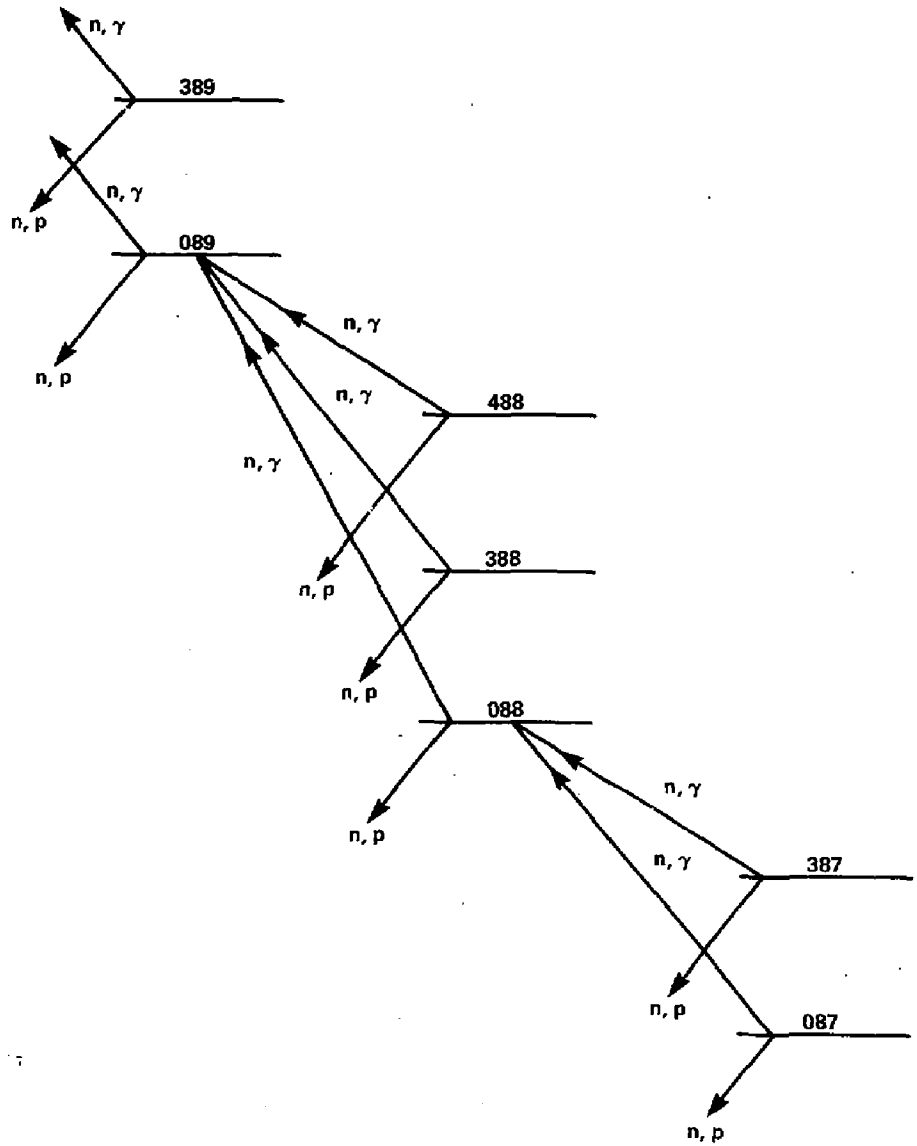

Figure 11

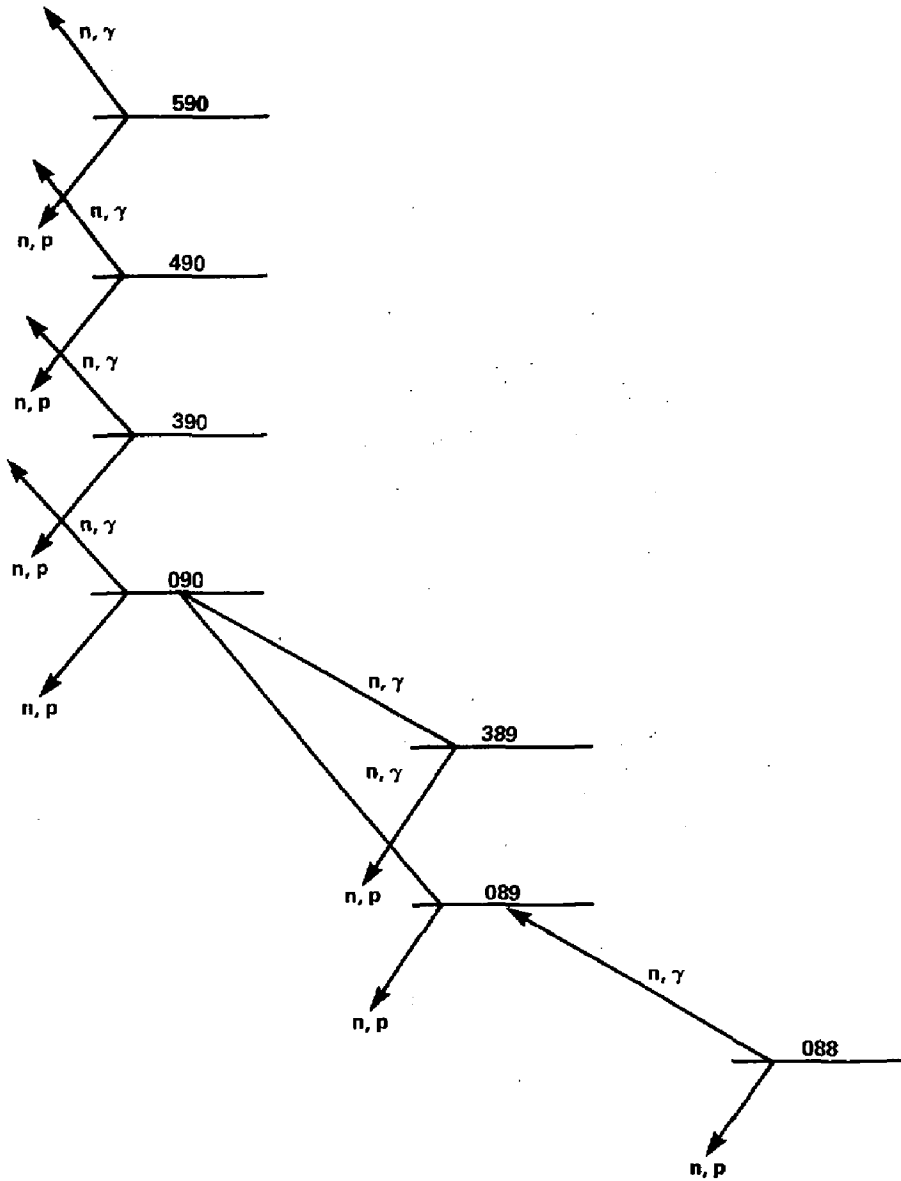

Figure 12

$$\frac{0.259}{389}$$

$$\frac{0.294}{089}\ \text{(Cross talk = +0.008)}$$

$$\frac{0.071}{488}$$

$$\frac{0.035}{388}$$

$$\frac{0.176}{088}\ \text{(Cross talk = +0.005)}$$

$$\frac{0.101}{387}$$

$$\frac{0.039}{087}$$

Figure 13

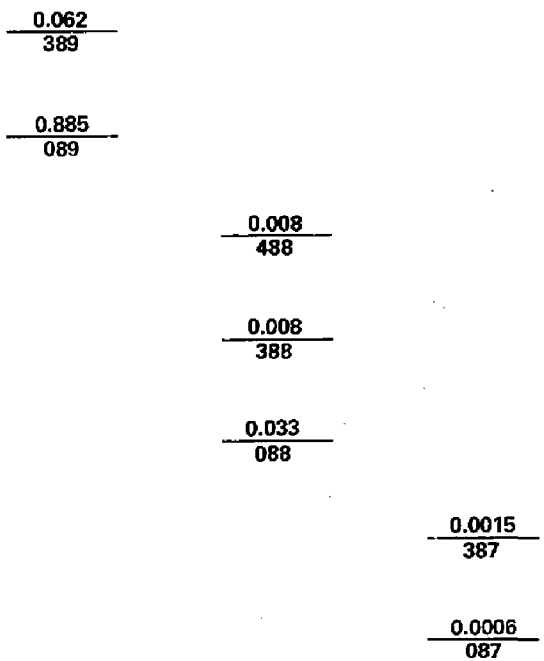
0.062
389
0.885
089
0.008
488
0.008
388
0.033
088
0.0015
387
0.0006
087

Figure 14

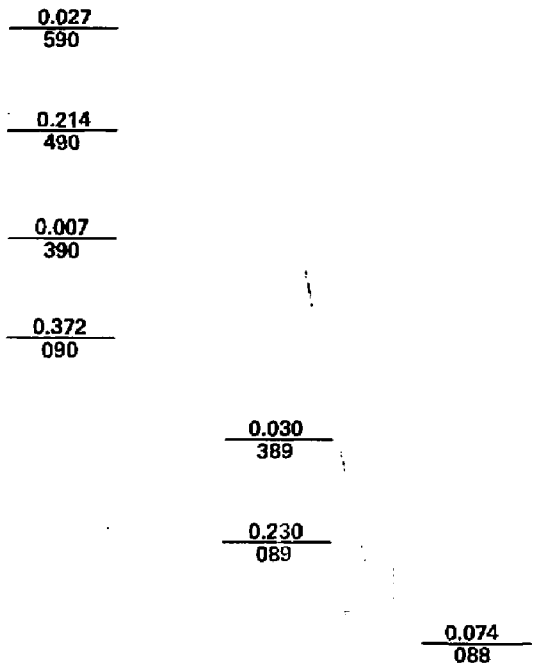

Figure 15

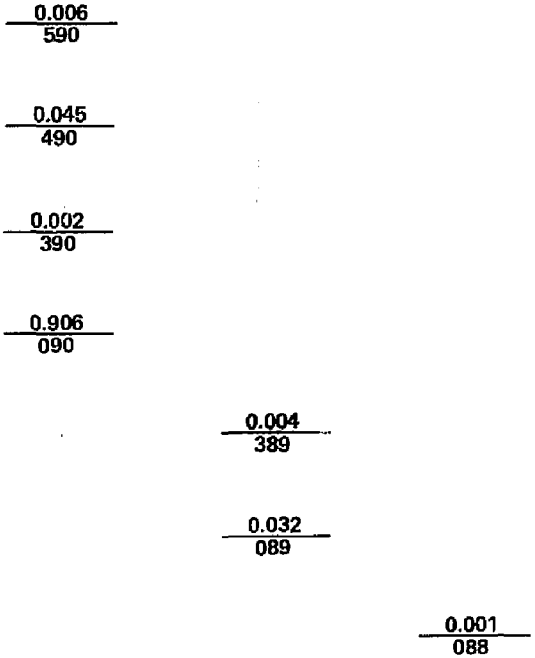

Figure 16